

# Multivariable control of modular multilevel converters with convergence and safety guarantees

Victor Daniel Reyes Dreke<sup>1</sup>, Ygor Pereira Marca<sup>2</sup>, Maurice Roes<sup>3</sup> and Mircea Lazar<sup>4</sup>

**Abstract**—Well-designed current control is a key factor in ensuring the efficient and safe operation of modular multilevel converters (MMCs). Even though this control problem involves multiple control objectives, conventional current control schemes are comprised of independently designed decoupled controllers, e.g., proportional-integral (PI) or proportional-resonant (PR). Due to the bilinearity of the MMC dynamics, tuning PI and PR controllers so that good performance and constraint satisfaction are guaranteed is quite challenging. This challenge becomes more relevant in an AC/AC MMC configuration due to the complexity of tracking the single-phase sinusoidal components of the MMC output. In this paper, we propose a method to design a multivariable controller, i.e., a static feedback gain, to regulate the MMC currents. We use a physics-informed transformation to model the MMC dynamics linearly and synthesise the proposed controller. We use this linear model to formulate a linear matrix inequality that computes a feedback gain that guarantees safe and effective operation, including (i) limited tracking error, (ii) stability, and (iii) meeting all constraints. To test the efficacy of our method, we examine its performance in a direct AC/AC MMC simulated in Simulink/PLECS and in a scaled-down AC/AC MMC prototype to investigate the ultra-fast charging of electric vehicles.

## I. INTRODUCTION

Modular multilevel converters (MMCs) are novel voltage source converters that offer high efficiency, scalability, and low harmonic distortion [1]–[4]. Well-designed current control is a key factor in ensuring their safe and efficient operation [5]. This control problem involves multiple control objectives, i.e., regulating the grid current, the MMC output current, and the sum of the capacitor voltages in each arm. In this case, regulating both currents controls the power transmitted from the grid to the MMC output. Furthermore, the safe operation depends mainly on stabilising the sum of the capacitor voltages of each arm, i.e., total arm voltage [6].

The conventional control schemes (CCSs) of the MMC currents, as defined in [5] and [6], consist of a set of independently designed controllers for each control objective. In this case, these controllers are usually single-input, single-output (SISO) controllers, such as proportional-integral (PI) or proportional-resonant (PR) controllers, which are not designed to deal with constrained multivariable control problems. As MMCs are multivariable systems with bilinear dynamics and

constrained control inputs, a major issue in the design of CCSs is tuning the controllers to ensure the desired performance, stability, and constraint satisfaction. Commonly, these tuning procedures are based on trial-and-error methods. As a consequence, when compared with multivariable control solutions as linear quadratic regulator (LQR) or model predictive control (MPC), the CCS's performance is lower (see e.g. [7]–[11]).

Furthermore, the complexity of the CCS depends on the waveform shape of the MMC output. For MMCs operating under AC outputs, i.e., AC/AC MMC, this complexity increases due to the challenges of tracking single-phase AC signals. A usual solution, i.e., PI, can stabilize sinusoidal signals as in [12]–[14], but they can not achieve zero error tracking. The alternative, i.e., PR, has a narrow frequency band around the resonance frequency. Hence, perturbations in the resonance frequency can reduce the controller performance dramatically [15].

Guaranteeing convergence of the controlled variables while meeting constraints is another of the challenges of the CCS. In [16], it is shown that using PI controllers can ensure MMC's safe operation, i.e., having stable total arm voltage. In this case, unconstrained continuous-time PIs used in AC/DC MMCs are considered. However, [16] does not discuss tuning methods or performance of the controllers. An alternative approach is multivariable control, i.e., state feedback gain [17], [18]. These solutions also use a linear model of the MMC in the dq-reference framework. Despite having better performance and being robust against model uncertainty, they are unconstrained and only compatible with AC/DC MMCs. Nowadays, MPC is the only implemented solution that offers high performance, convergence, and constraint satisfaction [3]. However, its use is minimal due to its computational complexity, especially in AC/AC MMCs [5].

In this paper, we propose a framework to design a multivariable controller, i.e., static feedback gain, to control the MMC currents in the *abc*-reference framework regardless of the configuration. We use a physics-informed transformation to model the MMC dynamics linearly and synthesise the proposed controller. Using linear matrix inequalities (LMIs) inspired by [19, Theorem 1 c.f.], we synthesise a controller that, in closed-loop with the linear model, reaches zero-error tracking while recursively meeting constraints inside a level set. This level set, i.e., an invariant domain of attraction, is a byproduct of the LMI. Moreover, we prove that, in a closed loop with the MMC, this controller guarantees a bounded tracking error of the MMC currents while keeping the total arm voltage stable, i.e., safe operation. We demonstrate

This research was funded by the NEON (New Energy and Mobility Outlook for the Netherlands) Crossover NWO (Dutch Research Council) Grant, project number 17628.

Affiliation: <sup>[1,4]</sup> Control Systems Group, Department of Electrical Engineering, Eindhoven University of Technology, The Netherlands. <sup>[2,3]</sup> Electromechanics and Power Electronics Group, Department of Electrical Engineering, Eindhoven University of Technology, The Netherlands. E-mails: <sup>1</sup> v.d.reyes.dreke@tue.nl, <sup>4</sup> m.lazar@tue.nl.

the controller efficacy in two scenarios: (i) simulation in a Simulink/PLECs environment and (ii) a scaled-down MMC prototype of direct AC/AC MMC for ultra-fast chargers.

### A. Basic Notation:

Let  $\mathbb{N}$ ,  $\mathbb{N}_+$ ,  $\mathbb{R}$ ,  $\mathbb{R}_+$ , and  $\mathbb{Z}$  denote the set of natural numbers, the set of natural numbers excluding 0, the field of real numbers, the field of non-negative real numbers and the set of integer numbers, respectively. For a set  $\mathbb{S} \subseteq \mathbb{R}^n$  define  $\mathbb{S}_{[a,b]} := \{s \in \mathbb{S} : a \leq s \leq b\}$ . Define an  $n$ -dimensional vector filled with ones as  $\mathbf{1}_n$  and one filled with zeros as  $\mathbf{0}_n$ . The identity matrix is denoted as  $\mathbf{I}_n$ . A block diagonal matrix with matrices  $A_1$  to  $A_m$  on the diagonal is denoted by  $\text{diag}(A_1, \dots, A_m)$ . For matrices  $A, B \in \mathbb{R}^{n \times m}$ , horizontal and vertical concatenation are defined as  $[A, B] = [A \ B]$  and  $[A; B] = [A^T \ B^T]^T$ , respectively.

We write  $A \succ 0$  ( $A \succeq 0$ ) for a symmetric, positive (semi)definite matrix  $A = A^T \in \mathbb{R}^{n \times n}$ . The  $i$  eigenvalues of a matrix  $A \in \mathbb{R}^{n \times n}$  are denoted by  $\lambda_i(A)$  and the spectral radius of  $A$  is  $\rho(A) := \max\{|\lambda_1(A)|, \dots, |\lambda_n(A)|\}$ . A discrete-time state-space model, i.e.,  $x(k+1) = Ax(k) + Bu(k)$ , is represented as  $x^+ = Ax + Bu$ , where  $x^+ := x(k+1)$  and  $x := x(k)$ .

## II. MMC AVERAGE MODELLING

A standard MMC is comprised of three-phase legs, labelled by  $m \in \{a, b, c\}$ , each of which consists of two arms, labelled by  $n \in \{u, l\}$  corresponding to the upper and lower arm, respectively. The arms are composed of  $N$  modules (SM) connected in series, an arm inductor ( $L_m$ ), and an arm resistance ( $R_m$ ) that models the conduction losses of the arm. This paper considers an MMC equivalent circuit as in [12], [20], see Figure 1. The arm current dynamics, i.e.,  $i_m^n$ , for all phases  $m \in \{a, b, c\}$  yields

$$L_m \frac{d}{dt} i_m^u + R_m i_m^u = u_m^u + v_m^g - v^z, \quad (1a)$$

$$L_m \frac{d}{dt} i_m^l + R_m i_m^l = u_m^l - v_m^g - v^z, \quad (1b)$$

with

$$u_m^n = \sum_{i=1}^N s_i^{\{n,m\}} \cdot v_{C_i}^{\{n,m\}}, \quad \forall n \in \{u, l\}, \quad (2a)$$

$$\frac{d}{dt} v_{C_i}^{\{n,m\}} = -\frac{1}{C_\gamma} s_i^{\{n,m\}} \cdot i_m^n, \quad \forall i \in \{1, \dots, N\}, \quad (2b)$$

where  $u_m^n \in \mathbb{R}$  is the arm voltage,  $C_\gamma \in \mathbb{R}_+$  is capacitance of the module, and for each  $i$  module,  $s_i^{\{n,m\}} \in \mathbb{Z}_{[-1,1]}$  is the switching signal,  $v_{C_i}^{\{n,m\}} \in \mathbb{R}_+$  is the capacitor voltage, and  $v^z$  and  $v_m^g$  are the output and the grid voltage, respectively. In this case, we can represent the grid and the MMC output currents as a linear combination of the arm currents, i.e.,

$$i_m^g = i_m^u - i_m^l \quad \text{and} \quad i^z = \sum_{m=\{a,b,c\}} i_m^z, \quad (3)$$

where, for all  $m \in \{a, b, c\}$ ,  $i_m^g$  are the grid currents and  $i_m^z := (i_m^u + i_m^l)/2$  are the MMC output currents per phase.

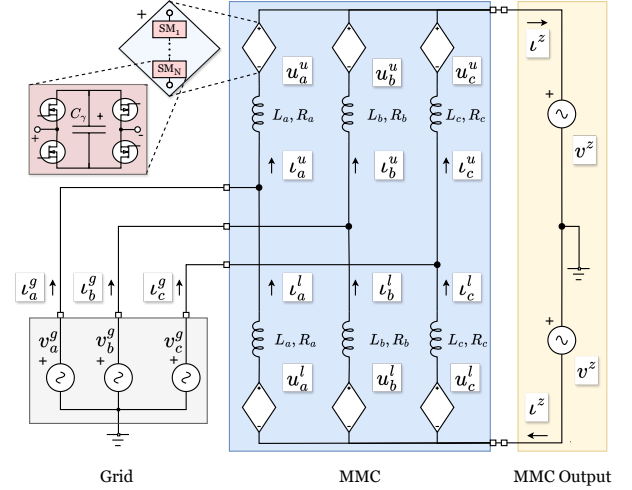


Fig. 1: Schematic of a three-phase bidirectional direct AC/AC MMC topology with full-bridge submodules as presented in [12].

The complexity and dimension of the model resulting from using (1) and (2) are high due to the bilinear influence of the integer control signal ( $s_i^{\{n,m\}}$ ). An accepted solution to reduce the model complexity and dimension is using the model approach as in [21], [22]. In these cases, it is assumed that the capacitor voltages are balanced in each arm  $n \in \{u, l\}$  for all the phases  $m \in \{a, b, c\}$ , such that

$$v_{C_i}^{\{n,m\}} = v_{C_j}^{\{n,m\}}, \quad \forall (i, j) \in \{1, \dots, N\}. \quad (4)$$

Consequently, the arm voltage, i.e.,  $u_m^n$ , yields

$$u_m^n = \eta_m^n v_m^n, \quad \forall n \in \{u, l\} \quad (5)$$

with

$$v_m^n = \sum_{i=1}^N v_{C_i}^{\{n,m\}}, \quad \text{and} \quad \eta_m^n = \frac{1}{N} \sum_{i=1}^N s_i^{\{n,m\}}, \quad (6)$$

where  $\eta_m^n \in \mathbb{R}_{[-1,1]}$  is the insertion index and  $v_m^n \in \mathbb{R}$  is the total arm voltage. As in [22], we approximate the insertion index to a continuous signal to remove the discontinuities.

Based on (1) and (5), let us define a state vector, i.e.,  $x = [x_a, x_b, x_c]^T \in \mathbb{R}^{12}$ , output vector, i.e.,  $y = [y_a, y_b, y_c]^T \in \mathbb{R}^6$ , insertion index vector, i.e.,  $\eta = [\eta_a, \eta_b, \eta_c]^T \in \mathbb{R}^6$ , and exogenous input vector, i.e.,  $w = [w_a, w_b, w_c, w_z]^T \in \mathbb{R}^8$ ; where for each phase  $m \in \{a, b, c\}$ , they are defined as

$$x_m = [i_m^u \ i_m^l \ v_m^u \ v_m^l], \quad y_m = [i_m^g \ i_m^z], \quad (7a)$$

$$\eta_m = [\eta_m^u \ \eta_m^l], \quad w_m = [v_m^g \ v_m^z], \quad (7b)$$

and

$$w_z = [v^z \ v^{z'}]. \quad (8)$$

In this case,  $i_m^g$  and  $i_m^z$  are the grid current and the output current, and  $v_m^g$  and  $v_m^z$  are obtained from the 90° phase delay of  $v_m^g$  and  $v_m^z$ , respectively. The resulting MMC bilinear

average model yields a discrete-time state-space model as follows

$$\begin{aligned} x^+ &= \mathbf{A}(\eta)x + \mathbf{E}w, \\ y &= \mathbf{C}x, \end{aligned} \quad (9)$$

with

$$\mathbf{A}(\eta) = \text{diag}\left(A(\eta_a^{u,l}), A(\eta_b^{u,l}), A(\eta_c^{u,l})\right), \quad (10a)$$

$$\mathbf{E} = [\text{diag}(E_a, E_b, E_c), E_z], \quad (10b)$$

$$\mathbf{C} = \text{diag}(C_a, C_b, C_c), \quad (10c)$$

where, for all phases  $m \in \{a, b, c\}$ ,

$$A(\eta_m^{u,l}) = \begin{bmatrix} K_1 & 0 & K_2\eta_m^u & 0 \\ 0 & K_1 & 0 & K_2\eta_m^l \\ K_3\eta_m^u & 0 & 1 & 0 \\ 0 & K_3\eta_m^l & 0 & 1 \end{bmatrix},$$

$$E_m = \begin{bmatrix} K_2 & 0 \\ -K_2 & 0 \end{bmatrix},$$

$$C_m = \begin{bmatrix} 1 & -1 & 0 & 0 \\ 0.5 & 0.5 & 0 & 0 \end{bmatrix},$$

and  $E_z = [-K_2\mathbf{1}_6 \quad \mathbf{0}_6]$ . The constants  $K_1=1 - \frac{R_m T_s}{L_m}$ ,  $K_2=\frac{T_s}{L_m}$ ,  $K_3=-\frac{NT_s}{C\gamma}$  were obtained by discretizing (1) with sampling time  $T_s$ , using the forward Euler method.

The complements of the grid and MMC output voltages, i.e.,  $v_m^{g'}$  and  $v^z$ , allow to model the dynamics of the exogenous inputs as an autonomous system, i.e.,

$$w^+ = \mathbf{S}w, \quad (12)$$

with  $\mathbf{S} = \text{diag}(\sigma(\omega_1 T_s), \sigma(\omega_1 T_s), \sigma(\omega_1 T_s), \sigma(\omega_2 T_s))$ , where  $\sigma(\cdot) : \mathbb{R} \rightarrow \mathbb{R}^{2 \times 2}$ , such that

$$\sigma(\omega T_s) = \begin{bmatrix} \cos(\omega T_s) & \sin(\omega T_s) \\ -\sin(\omega T_s) & \cos(\omega T_s) \end{bmatrix}, \quad (13)$$

$T_s \in \mathbb{R}$  is the sampling time,  $\omega_1 = 2\pi f_1 \in \mathbb{R}$  is the grid angular frequency, and  $\omega_2 = 2\pi f_2 \in \mathbb{R}$  is the MMC output angular frequency.

Albeit accurate, (9) is not commonly used when designing conventional control methods for the MMC [5], [6] due to the bilinear dynamics. A physics-informed transformation that simplifies (9) is to assume the arm voltages as the control inputs, i.e., disregard the capacitor voltage dynamics. Consequently, by defining a control input vector, i.e.,  $u = [u_a, u_b, u_c]^T$  with

$$u_m = [u_m^u \quad u_m^l], \quad \forall m \in \{a, b, c\}, \quad (14)$$

the total arm voltage dynamics are disregarded. This results in a reduced state vector, i.e.,  $\bar{x} = [\bar{x}_a, \bar{x}_b, \bar{x}_c]^T$  with

$$\bar{x}_m = [v_m^u \quad v_m^l], \quad \forall m \in \{a, b, c\}, \quad (15)$$

and in a linear state-space model, i.e.,

$$\begin{aligned} \bar{x}^+ &= \bar{\mathbf{A}}\bar{x} + \bar{\mathbf{B}}u + \mathbf{E}w, \\ y &= \bar{\mathbf{C}}\bar{x}, \end{aligned} \quad (16)$$

with

$$\bar{\mathbf{A}} = \text{diag}(\bar{A}_a, \bar{A}_b, \bar{A}_c), \quad (17a)$$

$$\bar{\mathbf{B}} = \text{diag}(\bar{B}_a, \bar{B}_b, \bar{B}_c), \quad (17b)$$

$$\bar{\mathbf{C}} = \text{diag}(\bar{C}_a, \bar{C}_b, \bar{C}_c), \quad (17c)$$

where for all phases  $m \in \{a, b, c\}$ ,

$$\bar{A}_m = \begin{bmatrix} K_1 & 0 \\ 0 & K_1 \end{bmatrix}, \quad B_m = \begin{bmatrix} K_2 & 0 \\ 0 & K_2 \end{bmatrix}, \quad (18a)$$

$$\bar{C}_m = \begin{bmatrix} 1 & -1 \\ 0.5 & 0.5 \end{bmatrix}. \quad (18b)$$

### III. MMC CONTROL PROBLEM DESCRIPTION

Figure 2 shows the most common hierarchical control scheme of MMCs [5]. This scheme has three stages: (i) current control, (ii) modulation, and (iii) voltage balancing, which are described in detail in [5], [6]. This paper focuses on the first stage, i.e., current control, which directly regulates the grid and the MMC output current as follows:

$$\lim_{k \rightarrow \infty} e_m^g := i_m^g(k) - i_m^{g*}(k) = 0, \quad \forall m \in \{a, b, c\}, \quad (19a)$$

$$\lim_{k \rightarrow \infty} e_m^z := i_m^z(k) - i_m^{z*}(k) = 0, \quad \forall m \in \{a, b, c\}, \quad (19b)$$

such that the desired per-phase power transfer is achieved, i.e.,

$$p_m^{g*} = v_m^g i_m^{g*}, \quad p_m^{z*} = 2v^z i_m^{z*}, \quad \forall m \in \{a, b, c\} \quad (20)$$

with

$$i_m^{g*} = \hat{I}_m^{g*} \cos(\omega_1 t + \phi_1), \quad v_m^g = \hat{V}_m^g \cos(\omega_1 t), \quad (21a)$$

$$i_m^{z*} = \hat{I}_m^{z*} \cos(\omega_2 t + \phi_2), \quad v^z = \hat{V}^z \cos(\omega_2 t), \quad (21b)$$

where  $p_m^{g*}$  and  $p_m^{z*}$  are the desired instantaneous power of the grid and transformer corresponding to the phase  $m$ ;  $\hat{I}_m^{g*}$ ,  $\hat{I}_m^{z*}$ ,  $\hat{V}_m^g$  and  $\hat{V}^z$  the peak-to-peak value of each corresponding variables; and  $\phi_1$  and  $\phi_2$  are the phase angle of the currents.

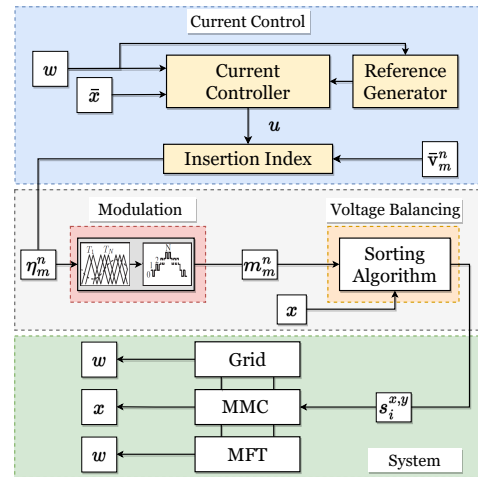


Fig. 2: Typical hierarchical control scheme of CCSs, as in [5], for MMCs connected to the grid and a medium frequency transformer (MFT).

To design the references  $i_m^{g*}$  and  $i_m^{z*}$ , we use the common- and differential-mode decomposition presented in [12], i.e.,

$$i_m^\Delta = \frac{i_m^u - i_m^l}{2}, u_m^\Delta = \frac{u_m^u - u_m^l}{2}, v_m^\Delta = \frac{v_m^u - v_m^l}{2}, \quad (22a)$$

$$i_m^\Sigma = \frac{i_m^u + i_m^l}{2}, u_m^\Sigma = \frac{u_m^u + u_m^l}{2}, v_m^\Sigma = \frac{v_m^u + v_m^l}{2}, \quad (22b)$$

where the superscripts  $\Delta$  and  $\Sigma$  label the differential and common-mode components, respectively. This decomposition decouples the dynamics of the grid and the MMC output currents, since  $i_m^g = 2i_m^\Delta$  and  $i_m^z = i_m^\Sigma$  [9], [12]. Using (22) and the MMC dynamics in (16), we propose a quadratic optimization problem to compute the optimal references. In this case, given  $i_m^\Delta$ , we can compute  $i_m^\Sigma$ , such that

$$\min_{i_m^\Sigma} \left\| \sum_{k=1}^{N_t(f_1)} \frac{(v_m^g(k) i_m^\Delta(k))}{N_t(f_1)} - \sum_{k=1}^{N_t(f_2)} \frac{(v_m^z(k) i_m^\Sigma(k))}{N_t(f_2)} \right\|, \quad (23a)$$

$$\text{s.t.} \quad \sum_{k=1}^{N_t(f_1)} \frac{(u_m^\Delta(k) i_m^\Delta(k))}{N_t(f_1)} + \sum_{k=1}^{N_t(f_2)} \frac{(u_m^\Sigma(k) i_m^\Sigma(k))}{N_t(f_2)} = 0, \quad (23b)$$

where  $N_t(f) = 1/fT_s \in \mathbb{N}$  is the number of samples in a period, i.e.,  $T = 1/f$ . Using the power equations in [23], we calculate  $i_m^{\Delta*}$  and assume that  $2i_m^{\Delta*} = i_m^{g*}$ . Since (23) considers the dynamics of (16), we compute an optimal  $i_m^\Sigma$ , i.e.,  $i_m^{\Sigma*}$ , which minimizes the power difference between grid and the MMC output while keeping the average of the arm power equal to zero. As explained in [12], imposing (23b) ensures stable dynamics of the total arm voltage, such that, for all phases  $m \in \{a, b, c\}$ ,

$$\sum_{j=1}^{N_T} v_m^\Delta(k+j) = 0, \text{ and } \sum_{j=1}^{N_T} v_m^\Sigma(k+j) = \hat{V}_m^g + \hat{V}_m^z. \quad (24)$$

Hence, by tracking these references, the current controller generates arm voltages that guarantee safe operation of the MMC. From (21), we infer the linear relationship between the exogenous inputs and the reference vector for the current controller, i.e.,  $r = [r_a, r_b, r_c]^\top$  with

$$r_m = [i_m^{g*} \ i_m^{z*}], \quad \forall m \in \{a, b, c\}, \quad (25)$$

such that

$$r = \mathbf{O}w \quad (26)$$

with  $\mathbf{O} = [\text{diag}(O_a, O_b, O_c), [O_z; O_z; O_z]]$ , where

$$O_m = \begin{bmatrix} o_1 & o_2 \\ 0 & 0 \end{bmatrix}, \quad \forall m \in \{a, b, c\}, \quad (27a)$$

$$O_z = \begin{bmatrix} 0 & 0 \\ o_3 & o_4 \end{bmatrix}. \quad (27b)$$

The coefficients of  $\mathbf{O}$  are  $o_1 = K_4 \cos(\phi_1)$ ,  $o_2 = -K_4 \sin(\phi_1)$ ,  $o_3 = K_5 \cos(\phi_2)$  and  $o_4 = -K_5 \sin(\phi_2)$  with  $K_4 = 2\hat{I}_m^{\Delta*}/\hat{V}_m^g$  and  $K_5 = \hat{I}_m^{\Sigma*}/\hat{V}_m^z$ , as in [23].

As in (16), the control input of the current controller is the arm voltage ( $u_m^n$ ). Thus, to transform the arm voltage into an insertion index, we use the formulation from [16], i.e.,

$$\eta_m^n = \text{sat} \left( \frac{u_m^n}{\hat{V}_m^g + \hat{V}_m^z} \right), \quad \forall n \in \{u, l\}, m \in \{a, b, c\} \quad (28)$$

with  $\text{sat}(\cdot) : \mathbb{R} \rightarrow \mathbb{R}_{[-1,1]}$ , i.e.,

$$\text{sat}(\xi) := \begin{cases} 1 & \text{if } \xi > 1 \\ \xi & \text{if } |\xi| \leq 1 \\ -1 & \text{if } \xi < -1 \end{cases}. \quad (29)$$

Using (23) will ensure the stabilising properties of (28) as we will show in the next sections.

#### IV. MIMO CURRENT CONTROL FOR MMC

In this section, we present a framework to design a multiple-input, multiple-output (MIMO) controller to track the currents of the MMC as in (19), while stabilising the total arm voltage as in (24). In this case, we aim to reach zero tracking error ( $e(k)$ ), such that

$$\lim_{k \rightarrow \infty} e(k) := y(k) - r(k) = 0, \quad (30)$$

while meeting performance and safety constraints, i.e.,

$$x(k) \in \mathcal{X} \subseteq \mathbb{R}^{12}, u(k) \in \mathcal{U} \subseteq \mathbb{R}^6 \quad \forall k \in \mathbb{N}. \quad (31)$$

Working in the  $abc$ -reference framework implies tracking time-varying references. Hence, the constraints are easily formulated as the error between the measurements and the ideal dynamics. In this paper, we define the ideal dynamics of the arm currents as the steady-state corresponding to reaching zero tracking error as in (30), i.e.,

$$\bar{x}^{ss+} = \bar{\mathbf{A}}\bar{x}^{ss} + \bar{\mathbf{B}}u^{ss} + \bar{\mathbf{E}}w, \quad (32)$$

where  $\bar{x}^{ss}$  is the reference steady-state, such that  $r = \bar{\mathbf{C}}\bar{x}^{ss}$  and  $u^{ss}$  is the steady-state of the control input. Then, let us define the state tracking error as

$$e_x(k) := \bar{x}(k) - \bar{x}^{ss}(k), \quad (33)$$

and control input tracking error as

$$e_u(k) := u(k) - u^{ss}(k). \quad (34)$$

Then, the controller must meet the error constraints, i.e.,

$$e_x(k) \in \mathbb{X} \text{ and } e_u(k) \in \mathbb{U}, \quad \forall k \in \mathbb{N}, \quad (35)$$

with

$$\mathbb{X} := \{e_x \in \mathbb{R}^6 : g_{t_x}^\top e_x \leq 1, \forall t_x \in \{1, \dots, s\}\}, \quad (36a)$$

$$\mathbb{U} := \{e_u \in \mathbb{R}^6 : h_{t_u}^\top e_u \leq 1, \forall t_u \in \{1, \dots, l\}\}. \quad (36b)$$

In this case,  $e_x(k) \in \mathbb{X} \implies x \in \mathcal{X}$  and  $e_u(k) \in \mathbb{U} \implies u \in \mathcal{U}$ , i.e., we define a bound for tracking the MMC arm currents such that the total arm voltage is also kept bounded within a certain operation region.

To design the proposed controller, we consider a compact representation of the MMC, grid and transformer described by (16) and (12), i.e.,

$$\bar{\Sigma} : \begin{cases} \bar{x}^+ = \bar{A}\bar{x} + \bar{B}u + Ew, \\ y = \bar{C}\bar{x}, \\ w^+ = Sw, \\ r = Ow, \end{cases} \quad (37)$$

In [19], the authors discussed an unconstrained solution for (30) when linear dynamics as in (16) are considered, i.e., the linear output tracking problem (LOTP). From [19], it is known that there exists a solution to the LOTP if the following assumption holds.

**Assumption IV.1 (Sylvester's equation for the LOTP [19])**

There exist matrices  $\Pi$  and  $\Gamma$  such that

$$\Pi S = A\Pi + B\Gamma + E, \quad (38a)$$

$$C\Pi = O, \quad (38b)$$

where  $A, B, C, E$ , are the matrices of the state space model of a linear system, and  $S$  and  $O$  are the matrices describing an autonomous exogenous system, as in (37).

**Theorem IV.2 (Controller Synthesis)** Suppose that Assumption IV.1 holds for system (37). Consider the following linear matrix inequalities:

$$\begin{bmatrix} Z & (\bar{A}Z + \bar{B}Y)^\top \\ (\bar{A}Z + \bar{B}Y) & Z \end{bmatrix} \succ 0, \quad (39a)$$

$$\forall t_x \in \{1, \dots, s\}, \begin{bmatrix} Z & (Zg_{t_x})^\top \\ (Zg_{t_x}) & 1 \end{bmatrix} \succcurlyeq 0, \quad (39b)$$

$$\forall t_u \in \{1, \dots, l\}, \begin{bmatrix} Z & (Yh_{t_u})^\top \\ (Yh_{t_u}) & 1 \end{bmatrix} \succcurlyeq 0, \quad (39c)$$

where the pair  $(\bar{A}, \bar{B})$  comes from (16),  $g_{t_x}$  and  $h_{t_u}$  are vectors corresponding to the error constraints from  $\mathbb{X}$  and  $\mathbb{U}$ , respectively. If there exist  $Y$  and  $Z$  such that (39) holds, then the closed-loop system comprised by (37) and the static feedback gain controller, i.e.,

$$u = K_x \bar{x} + K_w w, \quad (40)$$

where

$$K_x = YZ^{-1} \text{ and } K_w = \Gamma - K_x\Pi, \quad (41)$$

is asymptotically stable with a domain of attraction, i.e.,

$$\mathbb{S}_x = \{e_x \in \mathbb{R}^6 : e_x^\top P e_x \leq 1\} \subseteq \mathbb{X}, \quad (42)$$

where  $P = Z^{-1}$ , and the level set of feasible control inputs, i.e.,  $\mathbb{S}_u = K_x \mathbb{S}_x \subseteq \mathbb{U}$ .

*Proof:* From [19], it is known that given the pair  $(\Pi, \Gamma)$ , the steady-state dynamics are defined as

$$\bar{x}^{ss} = \Pi w, \text{ and } u^{ss} = \Gamma w \quad (43)$$

yields the ideal dynamics as in (32), where  $e(k) = \bar{C}\bar{x}^{ss}(k) - r(k) = 0$ , for all  $k \in \mathbb{N}$ . Using (33), (34), (37) and (43), we

derive the state tracking error dynamics and the control input error as follows

$$e_x^+ = (\bar{A} + \bar{B}K_x)e_x, \quad (44a)$$

$$e_u = K_x e_x. \quad (44b)$$

The full derivation of (44) can be founded in Appendix-A. Note that the LMIs (39) can be rewritten as:

$$(\bar{A} + \bar{B}K_x)^\top P (\bar{A} + \bar{B}K_x) \prec P, \quad (45a)$$

$$\forall t_x \in \{1, 2, \dots, s_i\}, \sqrt{g_{t_x}^\top P^{-1} g_{t_x}} \leq 1, \quad (45b)$$

$$\forall t_u \in \{1, 2, \dots, l_i\}, \sqrt{h_{t_u}^\top K_x P^{-1} K_x^\top h_{t_u}} \leq 1, \quad (45c)$$

where (45a)-(45c) are obtained by applying Schur complement, respectively. If (45) is feasible for a given  $\bar{A}, \bar{B}, g_{t_x}$  and  $h_{t_u}$ , then i)  $\rho(\bar{A} + \bar{B}K_x) < 1$  that implies that  $\lim_{k \rightarrow \infty} e_x(k) = 0$  and  $\lim_{k \rightarrow \infty} e_u(k) = 0$ , i.e., the state tracking error is asymptotically stable, and consequently, the LOTP is solved, ii)  $(\bar{A} + \bar{B}K_x)\mathbb{S}_x \subseteq \mathbb{S}_x$ , i.e.,  $\mathbb{S}_x$  is a positively invariant set, iii)  $\mathbb{S}_x \subseteq \mathbb{X}$ , i.e., the domain of attraction is constraint admissible iv)  $K_x \mathbb{S}_x \subseteq \mathbb{U}$ , i.e., the resulting level set is constraint admissible too. ■

**Remark IV.3** For Theorem IV.2, we assume that  $K_x$  is not given. However, to ensure certain error dynamics,  $K_x$  can be pre-calculated and then, solve the LMIs (39). The main difference with Theorem IV.2 is that the size of  $\mathbb{S}_x$  can be affected by  $K_x$ . This approach can boost MMC's performance, but it may reduce the domain of attraction.

**Remark IV.4** Employing the developed controller results in a structure of the current control as shown in Figure 3. This controller works in the  $abc$ -reference framework and only needs measurements of the grid and the MMC output voltages to align to their phases. In this case, we are not limited by the shape of the waveform as long as it can be modelled as a linear autonomous system as in (12). Moreover, the computational load is similar to the existent CCSs.

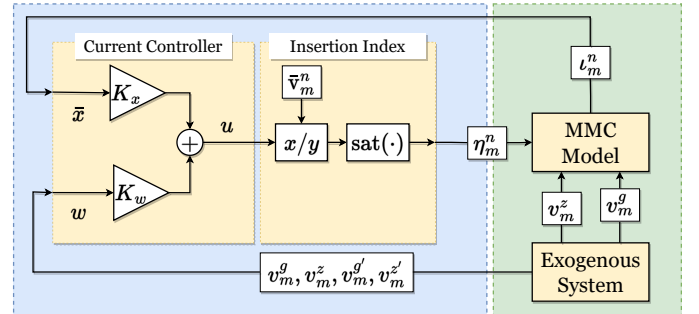


Fig. 3: Block diagram of the proposed MMC's Current Control

### A. Stability Guarantees

Theorem IV.2 proves the convergence and constraint satisfaction of the closed-loop system (37)-(40). However, (37) disregards the use of the insertion index and the dynamics of the total arm voltage ( $v_m^n$ ). Hence, we still need to ensure MMC stability, i.e., safe operation, when the controller (40) is used.

Let us consider an equivalent representation of (37), i.e., a bilinear model, such that

$$\tilde{\Sigma} : \begin{cases} \tilde{x}^+ = \tilde{\mathbf{A}}(\eta) \tilde{x} + \mathbf{E}w, \\ y = \mathbf{C}\tilde{x}, \\ w^+ = \mathbf{S}w, \\ r = \mathbf{O}w, \end{cases} \quad (46)$$

with  $\tilde{\mathbf{A}}(\eta) = \text{diag}(\tilde{A}(\eta_a^{u,l}), \tilde{A}(\eta_b^{u,l}), \tilde{A}(\eta_c^{u,l}))$ , and  $\tilde{x} = [\tilde{x}_a, \tilde{x}_b, \tilde{x}_c]^\top$ , where for all phases  $m \in \{a, b, c\}$ ,

$$\tilde{A}(\eta_m^{u,l}) = \begin{bmatrix} K_1 & 0 & K_2\eta_m^u & 0 \\ 0 & K_1 & 0 & K_2\eta_m^l \\ 0 & 0 & 1 & 0 \\ 0 & 0 & 0 & 1 \end{bmatrix}, \quad \text{and} \quad (47a)$$

$$\tilde{x}_m = [\iota_m^u \iota_m^l v_m^u v_m^l]^\top. \quad (47b)$$

In (46), we incorporate the bilinear dynamics caused by  $\eta$ . However, the total arm voltage has decoupled constant dynamics, i.e.,

$$v_m^n(k) = v_m^n(0), \quad \forall k \in \mathbb{N}_+. \quad (48)$$

Even when (46) is not physically accurate, it ensures that

$$\mathbf{C}\tilde{x} = \bar{\mathbf{C}}\bar{x} \quad \forall k \in \mathbb{N}. \quad (49)$$

Considering the references resulting from (23) and  $v_m^n(0) = \hat{V}_m^g + \hat{V}_m^z$  implies that the closed-loop system (40)-(46) tends to the ideal dynamics of the MMC presented in [6], [12]; i.e.,  $\lim_{k \rightarrow \infty} \tilde{x}_m(k) = x_m^*(k)$ , for all  $k \in \mathbb{N}$  with

$$x_m^*(k) = [\iota_m^{u*} \iota_m^{l*} v_m^u v_m^l], \quad \forall m \in \{a, b, c\} \quad (50)$$

where  $\iota_m^{u*} = \iota_m^{z*} + 0.5\iota_m^{g*}$ ,  $\iota_m^{l*} = \iota_m^{z*} - 0.5\iota_m^{g*}$ . So, the deviation between the MMC dynamics as (9) and the closed-loop system (40)-(46) determines the MMC stability.

**Definition IV.5 (MMC Safe Operation)** Let  $\mathcal{X} \subseteq \mathbb{R}^{12}$  be the constraint admissible set, i.e., safe operation region, and let  $\varepsilon(k) \in \mathbb{R}^{12}$  be the MMC deviation from the ideal dynamics, i.e.,

$$\varepsilon(k) := x(k) - \tilde{x}(k). \quad (51)$$

The MMC dynamics represented by (9) are stable if for any  $\gamma > 0$  there exist  $\delta = \delta(\gamma) > 0$  and  $\|\varepsilon(0)\| \leq \delta$  such that

$$\|\varepsilon(0)\| \leq \delta \implies \|\varepsilon(k)\| \leq \gamma, \quad \forall k \in \mathbb{N}_+, \quad (52)$$

where  $x(0) = \tilde{x}(0) \in \mathcal{X}$  are the initial states.

Based on (9) and (46), the MMC deviation dynamics, i.e.,  $\varepsilon^+ = x^+ - \tilde{x}^+$ , yield

$$\varepsilon^+ = \mathbf{A}(\eta)x - \tilde{\mathbf{A}}(\eta)\tilde{x}. \quad (53)$$

By adding and subtracting  $\mathbf{A}(\eta)\tilde{x}$ , (53) results in

$$\varepsilon^+ = \mathbf{A}(\eta)\varepsilon + \tilde{\mathbf{B}}(\eta)\tilde{x}, \quad (54)$$

where  $\tilde{\mathbf{B}}(\eta) = \mathbf{A}(\eta) - \tilde{\mathbf{A}}(\eta)$ . Note that (54) is a linear parameter-varying (LPV) representation, where  $\eta \in \Xi \subseteq \mathbb{R}_{[-1,1]}^6$  is the scheduling-variable, with  $\Xi$  being a closed polyhedron that contains the origin in its interior. Hence, using the LPV framework, we can analyse the stability of (54), which implies the safe operation of the MMC, as explained in Definition IV.5.

**Theorem IV.6 (MMC Stability)** Consider the system (54) with the scheduling-variable  $\eta \in \Xi \subseteq \mathbb{R}_{[-1,1]}^6$ . Let us define a Lyapunov candidate function  $V(\varepsilon)$ , i.e.,  $V(\varepsilon) := \varepsilon^T \mathbf{Q} \varepsilon$ . If there exists a matrix  $\mathbf{Q} \succ 0$  such that following inequality

$$\begin{bmatrix} \mathbf{Q} & \mathbf{Q}\mathbf{A}(\xi^i) \\ \mathbf{A}(\xi^i)^\top \mathbf{Q} & \mathbf{Q} \end{bmatrix} \succ 0, \quad (55)$$

is satisfied for all vertices  $\xi^i$  of  $\Xi$ , then (52) is satisfied, i.e., the MMC operation is stable, as in Definition IV.5.

*Proof:* Consider (54), i.e., a linear parameter-varying (LPV) system, as

$$\varepsilon^+ = \mathbf{A}(\eta)\varepsilon + \tilde{\mathbf{B}}(\eta)\tilde{x}. \quad (56)$$

Notice that in (54),  $\mathbf{A}(\eta)$  and  $\tilde{\mathbf{B}}(\eta)$  are affine in  $\eta$ . Hence, in this case, proving the quadratic stability of (54) implies robust stability; see [24] for proof. The quadratic stability of (54) is determined by the following inequalities:

$$\begin{aligned} \mathbf{A}(\eta)^\top \mathbf{Q} \mathbf{A}(\eta) - \mathbf{Q} &< 0, \quad \forall \eta \in \Xi, \\ \mathbf{Q} &\succ 0. \end{aligned} \quad (57)$$

Since  $\Xi$  is a convex set, inequality (57) is satisfied if

$$\begin{aligned} \mathbf{A}(\xi^i)^\top \mathbf{Q} \mathbf{A}(\xi^i) - \mathbf{Q} &< 0, \\ \mathbf{Q} &\succ 0, \end{aligned} \quad (58)$$

holds for all vertices  $\xi^i$  of  $\Xi$ . Then, applying Schur complement, (58) yields

$$\begin{bmatrix} \mathbf{Q} & \mathbf{Q}\mathbf{A}(\xi^i) \\ \mathbf{A}(\xi^i)^\top \mathbf{Q} & \mathbf{Q} \end{bmatrix} \succ 0, \quad (59)$$

for all vertices  $\xi^i$  of  $\Xi$ . ■

## V. SIMULATIONS RESULTS

To validate the performance of the proposed controller, we study its closed-loop response, considering two scenarios: (i) an average equivalent circuit of the MMC simulated in PLECS/Simulink equivalent to (9) and (ii) a linear average model equivalent to (16). In both cases, we use a direct AC/AC MMC to interface a medium-frequency transformer (MFT) for ultra-fast chargers with a medium-voltage grid, as in [12]. The MMC parameters are  $C_\gamma=4\text{mF}$ ,  $L_m=3\text{mH}$  and  $R_m=50\text{m}\Omega$ , and Table I shows its nominal operation during vehicle-to-grid (V2G) mode.

In this case, we apply Theorem IV.2 to find a controller that maintains the MMC within a safe region of operation, i.e.,

Nominal Value	Notation	Grid	MFT
Active Power	$P_m^g$	1MW	1MW
Voltage	$[\hat{V}_m^g, \hat{V}^z]$	25kV	10kV
Current	$[\hat{i}_m^g, \hat{i}_m^z]$	80A	101.15A
Frequency	$[f_1, f_2]$	50Hz	1kHz

TABLE I: Power requirements of the MMC in the Simulink environment.

$-0.1\bar{x}_{\text{nom}} \leq e_x \leq 0.1\bar{x}_{\text{nom}}$  and  $-0.08u_{\text{nom}} \leq e_u \leq 0.08u_{\text{nom}}$ , where  $\bar{x}_{\text{nom}} = \hat{i}_m^g + \hat{i}_m^z$  and  $u_{\text{nom}} = \hat{V}_m^g + \hat{V}^z$ . The resulting controller with a structure as (40) yields

$$K_x = \text{diag}(K_x^a, K_x^b, K_x^c), \quad (60a)$$

$$K_w = [\text{diag}(K_w^a, K_w^b, K_w^c), [K_w^z; K_w^z; K_w^z]], \quad (60b)$$

where, for each phase  $m \in \{a, b, c\}$ ,

$$K_x^m = -148.62\mathbf{I}_2, K_w^m = \begin{bmatrix} -0.7621 & -0.0015 \\ 0.7621 & 0.0015 \end{bmatrix},$$

and

$$K_w^z = \begin{bmatrix} 2.4919 & -0.1902 \\ 2.4919 & -0.1902 \end{bmatrix}.$$

Moreover, to assess the MMC stability, the solution from (55) of Theorem IV.6 yields  $Q \succ 0$ , i.e.,  $Q = \text{diag}(Q, Q, Q)$  with

$$Q = \begin{bmatrix} 1.582 & -0.437 & -0.449 & -0.437 \\ -0.437 & 1.583 & -0.437 & -0.449 \\ -0.449 & -0.437 & 1.583 & -0.437 \\ -0.437 & -0.449 & -0.437 & 1.583 \end{bmatrix}. \quad (61)$$

Figure 4 shows the simulation results corresponding to scenario (i). In Figure 4(a)-(b), we observe the tracked currents with the amplitude expected in Table I. The FFT analysis in Figure 4(c)-(d) shows a well-designed decoupling of the output currents, confirming the suitability of (60). Both currents, i.e., the grid current and the output current, have only visible components at their corresponding fundamental frequencies  $f_1$  and  $f_2$ , respectively.

Figure 5 shows the deviation of the MMC currents as (19), i.e.,  $\varepsilon_{\{1,2,5,6,9,10\}}$ , resulting from scenario (i). As expected from Theorem IV.6, the deviation is stable and bounded; see Figure 5(a)-(b). The FFT analysis of the tracking error shows some small components at 50Hz and 1kHz corresponding to the grid and output current, respectively. Hence, Figure 5(c)-(d) also confirms the good alignment to the grid and the MFT phases. We also observe some components in other frequencies, but the amplitude is relatively small, i.e.,  $< 0.125\%$ .

Figure 6 depicts the behaviour of the total arm voltage when scenario (i) was simulated. In Figure 6(a)-(b), the total arm voltage in the differential and common modes shows that the MMC is operating stably. The FFT analysis in Figure 6(c) proves that the total arm voltage ripples ( $\leq 0.1\%$ ) have components in the expected frequencies, as it was explained in [25].

We evaluate the design of the controller through the state tracking error dynamics corresponding to the simulated scenario (ii). For simplicity, in Figure 7, we plot the projection of

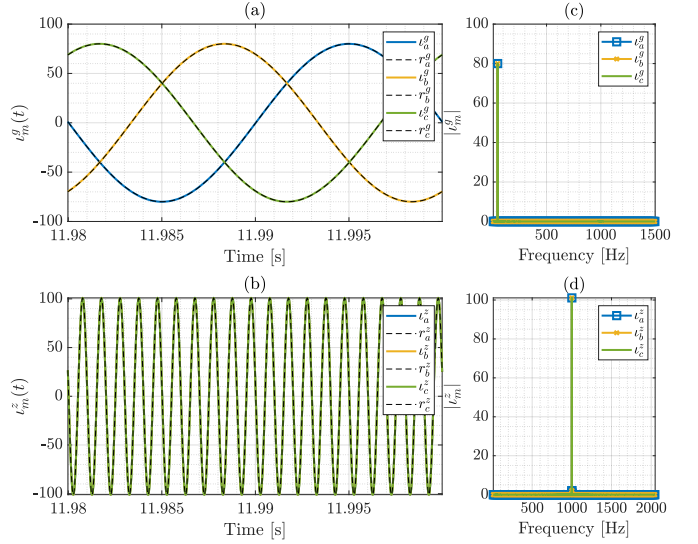


Fig. 4: Simulation results from scenario (i): (a) Trajectory of the grid current, (b) trajectory of the output current, (c) FFT analysis of grid current, and (d) FFT analysis output current.

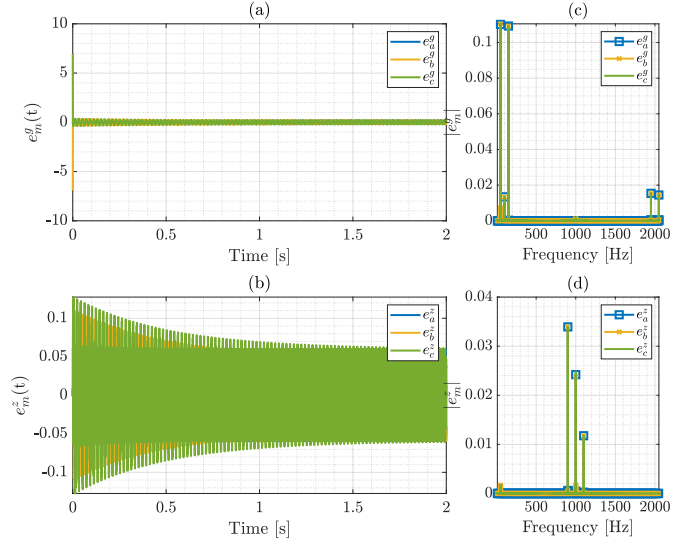


Fig. 5: Simulation results from scenario (i): (a) Error of the grid current  $e_m^g$ , (b) Error of the output current  $e_m^z$ , (c) FFT analysis of grid current error, and (d) FFT analysis output current error.

$\mathbb{S}_x$  corresponding to phases b and c. Note that for all  $k \in \mathbb{N}$ ,  $e_x(k) \in \mathbb{S}_x \subseteq \mathbb{X}$  and  $e_u(k) \in \mathbb{S}_u \subseteq \mathbb{U}$ .

## VI. EXPERIMENTAL VERIFICATION

The proposed controller is verified with a scaled-down prototype, shown in Figure 8. The experimental setup implements an AC/AC MMC to interface a three-phase voltage source, i.e., the grid simulator, with a medium-frequency transformer (MFT) primary side. The MMC is composed of PEH2015 and PEB8038 modules from Imperix. The system is controlled using four Imperix B-Box RCP 3.0 fast prototyping control

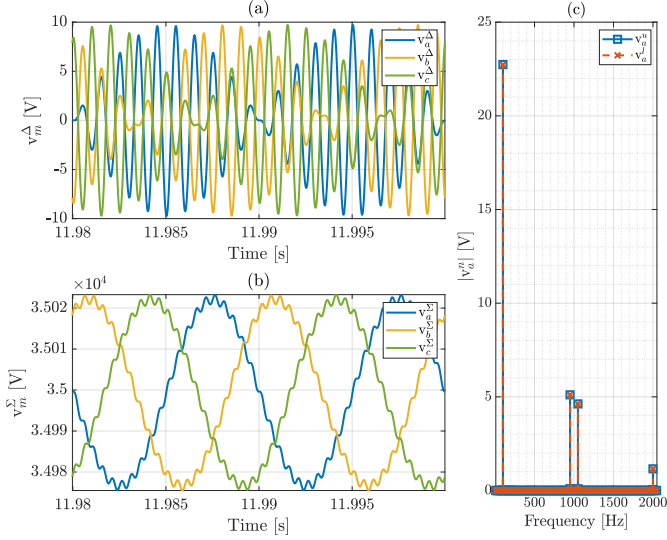


Fig. 6: Simulation results from scenario (i): (a) Trajectory of the differential-mode total arm voltage, (b) trajectory of the common-mode total arm voltage, (c) FFT analysis of the total arm voltage of phase a.

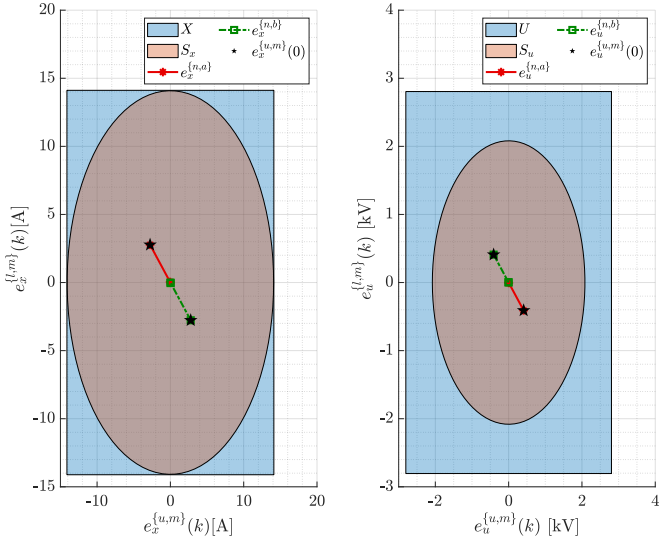


Fig. 7: Simulation results from scenario (ii) with initial condition ( $\star e(0)$ ): (a) Trajectory of the state tracking error  $e_x$ , operation region  $S_x$  and constraint  $X$ ; (b) trajectory of the control input tracking error  $e_u$ , operation region  $S_u$  and constraint  $U$ .

platform modules, which run the control scheme described in Section IV in discrete-time implementation. In addition, the data acquired via the controllers has a sample rate ( $T_s$ ) of 50 kHz. The MMC parameters are  $N=4$ ,  $C_\gamma=5\text{mF}$ ,  $L_m=2.36\text{mH}$  and  $R_m=50\text{m}\Omega$  and Table II shows its nominal operation during vehicle-to-grid (V2G) mode.

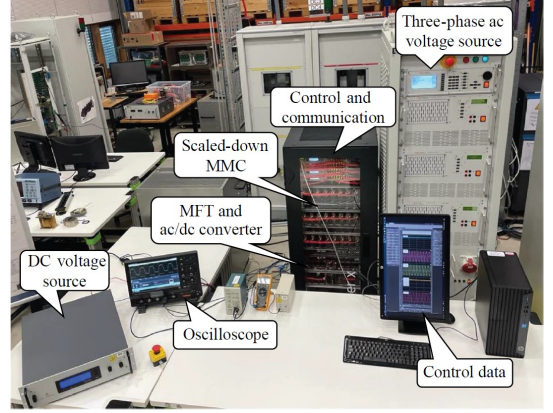


Fig. 8: Photograph of the experimental setup with the scaled-down MMC.

Nominal Value	Notation	Grid	MFT
Active Power	$P_m^g$	1/3 kW	1/3 kW
Voltage	$[\hat{V}_m^g, \hat{V}^z]$	300V	150V
Current	$[\hat{I}_m^g, \hat{I}_m^{z*}]$	3.33A	3.395A
Frequency	$[f_1, f_2]$	50Hz	1kHz

TABLE II: Power requirements of the AC/AC scaled-down prototype.

In this case, we apply Theorem IV.2 to find a controller that maintains the MMC within a safe region of operation, i.e.,  $-0.1\bar{x}_{\text{nom}} \leq e_x \leq 0.1\bar{x}_{\text{nom}}$  and  $-0.08u_{\text{nom}} \leq e_u \leq 0.08u_{\text{nom}}$ , where  $\bar{x}_{\text{nom}} = \hat{I}_m^g + \hat{I}_m^{z*}$  and  $u_{\text{nom}} = \hat{V}_m^g + \hat{V}^z$ . The resulting controller with a structure as (40) yields

$$K_x = \text{diag}(K_x^a, K_x^b, K_x^c), \quad (62a)$$

$$K_w = [\text{diag}(K_w^a, K_w^b, K_w^c), [K_w^z, K_w^z, K_w^z]], \quad (62b)$$

where, for each phase  $m \in \{a, b, c\}$ ,

$$K_x^m = -8.9465\mathbf{I}_2, K_w^m = \begin{bmatrix} -0.95 & -0.0040 \\ 0.95 & 0.0040 \end{bmatrix},$$

and

$$K_w^z = \begin{bmatrix} 1.1835 & -0.3265 \\ 1.1835 & -0.3265 \end{bmatrix}.$$

Moreover, to assess the MMC stability, the solution from (55) of Theorem IV.6 yields  $Q \succ 0$ , i.e.,  $Q = \text{diag}(Q, Q, Q)$  with

$$P = \begin{bmatrix} 1.582 & -0.437 & -0.448 & -0.437 \\ -0.437 & 1.582 & -0.437 & -0.449 \\ -0.448 & -0.437 & 1.582 & -0.437 \\ -0.437 & -0.448 & -0.437 & 1.582 \end{bmatrix}. \quad (63)$$

Figure 9 shows steady-state dynamics of the MMC output currents. By assessing Figure 9(a)-(b) and Figure 9(c)-(d), we



observe that the tracked currents have the amplitude expected in Table I. As in previous examples, the FFT analysis in Figure 9(c)-(d) shows a well-designed decomposition of the output currents, validating the suitability of (60).

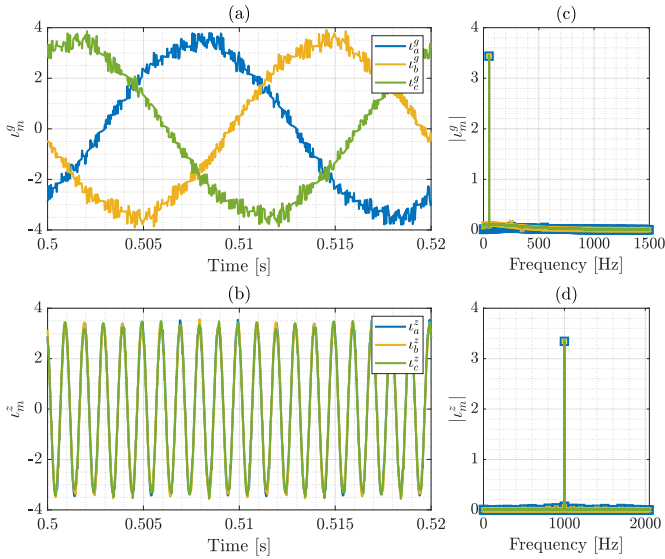


Fig. 9: (a) Steady-state trajectory of the grid currents, (b) Steady-state trajectory of the transformer currents, (c) FFT analysis of grid currents, and (d) FFT analysis transformer currents.

These output currents are generated by the insertion index presented in Figure 10. In this case, the insertion index remains between the intended operating region, while providing a good performance. Additionally, the FFT shows only components at the desired frequencies, i.e.,  $f_1$  and  $f_2$ . The amplitude corresponding to these frequencies also follows the MMC ideal dynamics expressed in [12].

Figure 11 depicts the behaviour of the differential and common modes of the total arm voltage. Note that the black dashed lines represent the average value of both signals. In this case, as in (24), the average value of the differential mode is equal to zero. The average of the common mode is not exactly  $\hat{V}_m^g + \hat{V}^z$  as in (24). This was expected due to the model mismatching, yet it does not compromise the stable and efficient operation of the MMC.

## VII. CONCLUSION

In this paper, we propose a controller for tracking the MMC currents while keeping the stored capacitor voltage stable. As an outcome of this paper, we provide evidence that a synthesized feedback gain is suitable for controlling the MMC. The static feedback gain is designed to achieve the required closed-loop performance while maintaining stability and safety. Moreover, the complexity of the proposed control scheme is simpler since no PLL is needed. Evidence of the advantage of the proposed controller is shown in different scenarios (i) linear average model, (ii) average equivalent MMC circuit, and (iii) prototype scaled-down MMC.

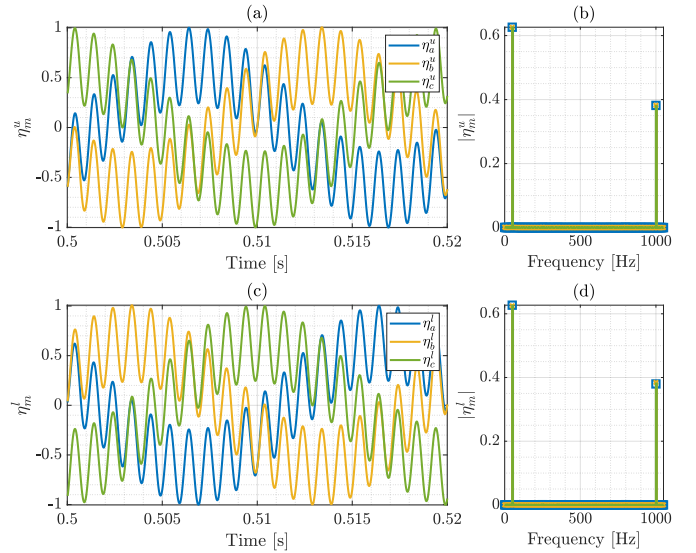


Fig. 10: (a) Steady-state trajectory of the insertion index of the upper arms, (b) Steady-state trajectory of the insertion index of the lower arms, (c) FFT analysis of the insertion index of the upper arms, and (d) FFT analysis of the insertion index of the lower arms.

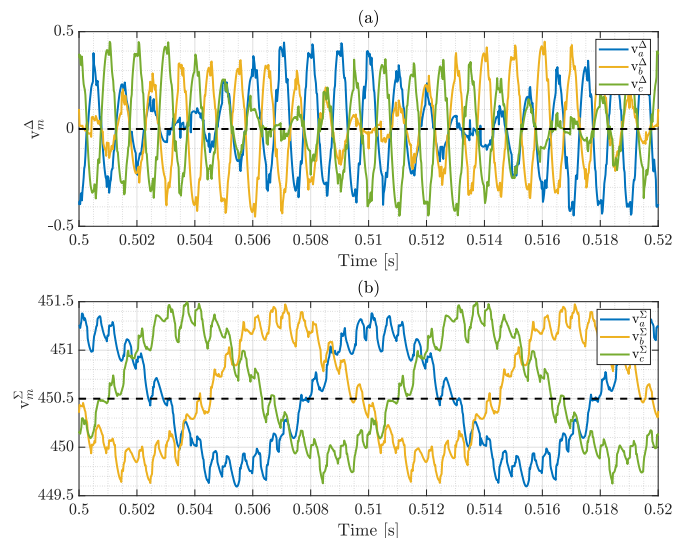


Fig. 11: (a) Steady-state trajectory of the differential-mode total arm voltage, (b) Steady-state trajectory of the common-mode total arm voltage,

## ACKNOWLEDGMENT

The authors would like to thank Jorge L. Duarte and Korneel G. E. Wijnands for sharing the topology of the modular multilevel converter for ultra-fast charging stations and for their useful comments.

### A. State and Control Input Error Dynamics

Recalling [19, Theorem 1 c.f.], let assume that there exist  $\Pi$  and  $\Gamma$  such that

$$\begin{aligned}\Pi S &= A\Pi + B\Gamma + E, \\ C\Pi &= O.\end{aligned}\quad (64)$$

Then, by multiplying the exogenous input vector, (64) yields

$$\begin{aligned}\Pi Sw &= A\Pi w + B\Gamma w + Ew, \\ C\Pi w &= Ow.\end{aligned}\quad (65)$$

Note that (65) confirms that defining the steady-state as

$$x^{ss} := \Pi w \quad \text{and} \quad u^{ss} := \Gamma w \quad (66)$$

guarantees that the tracking error is equal to zero, i.e.,

$$e(k) = Cx(k) - Ow(k) = 0. \quad (67)$$

Equation (65) can be re-written as

$$\Pi w(k+1) = A\Pi w + B\Gamma w + Ew \quad (68)$$

and, consequently, as

$$x^{ss}(k+1) = Ax^{ss} + Bx^{ss} + Ew. \quad (69)$$

By defining  $e_x = x - x^{ss}$ , and  $e_u = u - u^{ss}$ , it follows immediately that

$$\begin{aligned}e_x(k+1) &= x(k+1) - x^{ss}(k+1), \\ &= Ax(k) + Bu(k) + Ew(k) - \Pi Sw.\end{aligned}\quad (70)$$

Substituting (40) in (70), it yields

$$e_x(k+1) = (A+BK_x)x + (BK_w)w - (A\Pi+B\Gamma)w. \quad (71)$$

Rearranging (71) the error state dynamics is defined by an autonomous system, i.e.,

$$\begin{aligned}e_x(k+1) &= (A+BK_x)(e_x + \Pi w) + \\ &\quad (BK_w)w - (A\Pi+B(K_w+K_x\Pi))w \\ &= Ae_x(k) + BK_x e_x(k).\end{aligned}\quad (72)$$

From (72), the control input corresponding to state error yields  $e_u := K_x e_x$ , i.e.,

$$e_u = K_x(x - x^{ss}). \quad (73)$$

Note that (73) is equivalent to the control input error definition, i.e.,  $e_u = u - u^{ss}$  as in (34), since  $u^{ss} = \Gamma w$  and

$$u = K_x x + \underbrace{(\Gamma - K_x \Pi)}_{K_w} w. \quad (74)$$

- [1] A. Lesnicar and R. Marquardt, "An innovative modular multilevel converter topology suitable for a wide power range," in *2003 IEEE Bologna Power Tech Conference Proceedings*, vol. 3, 2003, pp. 6 pp. Vol.3-.
- [2] M. A. Perez, S. Ceballos, G. Konstantinou, J. Pou, and R. P. Aguilera, "Modular multilevel converters: Recent achievements and challenges," *IEEE Open Journal of the Industrial Electronics Society*, vol. 2, pp. 224–239, 2021.
- [3] R. V. K. Challa, S. Mikkili, and P. K. Bonthagorla, "Modeling, controlling approaches, modulation schemes, and applications of modular multilevel converter," *Journal of Control, Automation and Electrical Systems*, vol. 34, no. 1, pp. 189–215, 2023.
- [4] R. Marquardt, "Modular multilevel converters: State of the art and future progress," *IEEE Power Electronics Magazine*, vol. 5, no. 4, pp. 24–31, 2018.
- [5] S. Du, A. Dekka, B. Wu, and N. R. Zargari, *Modular Multilevel Converter: Analysis, Control and Applications*, T. Samad, Ed. John Wiley and Sons, 2018.
- [6] K. Sharifabadi, L. Harnefors, H. P. Nee, S. Norrga, and R. Teodorescu, *Design, control and application of modular multilevel converters for HVDC transmission systems*, 1st ed. John Wiley and Sons, Inc., 2016.
- [7] A. Dekka, B. Wu, V. Yaramasu, R. L. Fuentes, and N. R. Zargari, "Model predictive control of high-power modular multilevel converters—an overview," *IEEE Journal of Emerging and Selected Topics in Power Electronics*, vol. 7, pp. 168–183, 3 2019.
- [8] J. Böcker, B. Freudenberg, A. The, and S. Dieckerhoff, "Experimental comparison of model predictive control and cascaded control of the modular multilevel converter," *IEEE Transactions on Power Electronics*, vol. 30, no. 1, pp. 422–430, 2015.
- [9] M. Jeong, S. Fuchs, and J. Biela, "High performance lqr control of modular multilevel converters with simple control structure and implementation," in *2020 22nd European Conference on Power Electronics and Applications (EPE'20 ECCE Europe)*, 2020, pp. P.1–P.10.
- [10] G. Darivianakis, T. Geyer, and W. van der Merwe, "Model predictive current control of modular multilevel converters," in *2014 IEEE Energy Conversion Congress and Exposition (ECCE)*, 2014, pp. 5016–5023.
- [11] V. D. Reyes Dreke and M. Lazar, "Long-horizon nonlinear model predictive control of modular multilevel converters," *Energies*, vol. 15, no. 4, 2022.
- [12] Y. Pereira Marca, M. Roes, J. Duarte, and C. Wijnands, "Isolated mmc-based ac/ac stage for ultrafast chargers," in *2021 IEEE 30th International Symposium on Industrial Electronics (ISIE)*, 2021.
- [13] S. Song, J. Liu, S. Ouyang, X. Chen, and B. Liu, "Control of direct ac/ac modular multilevel converter in railway power supply system," in *2018 International Power Electronics Conference (IPEC-Niigata 2018 -ECCE Asia)*, 2018, pp. 1051–1055.
- [14] J. Yu, X. Hou, C. Xia, G. You, and Z. Liu, "Control method of an ac-ac mmc for open-end stator winding wind turbine generation system," *International Journal of Electrical Power and Energy Systems*, vol. 153, p. 109268, 2023.
- [15] A. Timbus, M. Ciobotaru, R. Teodorescu, and F. Blaabjerg, "Adaptive resonant controller for grid-connected converters in distributed power generation systems," in *Twenty-First Annual IEEE Applied Power Electronics Conference and Exposition, 2006. APEC '06.*, 2006, pp. 6 pp.–.
- [16] L. Harnefors, A. Antonopoulos, K. Ilves, and H.-P. Nee, "Global asymptotic stability of current-controlled modular multilevel converters," *IEEE Transactions on Power Electronics*, vol. 30, no. 1, pp. 249–258, 2015.
- [17] A. Zama, A. Benchaib, S. Bacha, D. Frey, S. Silvant, and D. Georges, "Linear feedback dead-beat control for modular multilevel converters: Validation under faults grid operation mode," *IEEE Transactions on Industrial Electronics*, vol. 68, no. 4, pp. 3181–3191, 2021.
- [18] S. D. Tavakoli, S. Fekriasl, E. Prieto-Araujo, J. Beerten, and O. Gomis-Bellmunt, "Optimal  $\mathcal{H}_\infty$  control design for mmc-based hvdc links," *IEEE Transactions on Power Delivery*, vol. 37, no. 2, pp. 786–797, 2022.
- [19] B. Francis and W. Wonham, "The internal model principle of control theory," *Automatica*, vol. 12, no. 5, pp. 457–465, 1976.
- [20] Y. Pereira Marca, J. Duarte, M. Roes, and C. Wijnands, "Extended operating region of modular multilevel converters using full-bridge sub-modules," in *2021 23rd European Conference on Power Electronics and Applications (EPE'21 ECCE Europe)*, 2021.

- [21] A. Lopez, D. E. Quevedo, R. Aguilera, T. Geyer, and N. Oikonomou, "Reference design for predictive control of modular multilevel converters," in *2014 4th Australian Control Conference (AUCC)*, 2014, pp. 239–244.
- [22] S. Rohner, J. Weber, and S. Bernet, "Continuous model of modular multilevel converter with experimental verification," in *2011 IEEE Energy Conversion Congress and Exposition*, 2011, pp. 4021–4028.
- [23] IEEE, "IEEE standard definitions for the measurement of electric power quantities under sinusoidal, nonsinusoidal, balanced, or unbalanced conditions," *IEEE Std 1459-2010 (Revision of IEEE Std 1459-2000)*, pp. 1–50, 2010.
- [24] G. S. Becker, *Quadratic stability and performance of linear parameter dependent systems*. University of California, Berkeley, 1993.
- [25] Y. Pereira Marca, M. Roes, and K. Wijnands, "Capacitor voltage ripple and capacitance evaluation in a direct three-phase to single-phase ac/ac mmc," in *11th International Conference on Power Electronics, ICPE 2023 ECCE*, 2023.